AGU PUBLICATIONS

JGR

Journal of Geophysical Research: Space Physics

RESEARCH ARTICLE

10.1002/2014JA020203

Key Points:
- Sensitivity of S and L to solar activity is shown to be comparable
- Both S and L scale with the square root of F10.7
- A long-term decrease in L is revealed

Correspondence to:
Y. Yamazaki,
y.yamazaki@lancaster.ac.uk

Citation:
Yamazaki, Y., and M. J. Kosch (2014), Geomagnetic lunar and solar daily variations during the last 100 years, *J. Geophys. Res. Space Physics*, *119*, doi:10.1002/2014JA020203.

Received 21 MAY 2014
Accepted 22 JUL 2014
Accepted article online 25 JUL 2014

Geomagnetic lunar and solar daily variations during the last 100 years

Y. Yamazaki[1] and M. J. Kosch[1,2]

[1]Department of Physics, Lancaster University, Lancaster, UK, [2]South African National Space Agency, Hermanus, South Africa

Abstract This paper describes long-term changes in the geomagnetic lunar (*L*) and solar (*S*) daily variations. We analyze the eastward component of the geomagnetic field observed at eight midlatitude stations during 1903–2012. The amplitude and phase for the semidiurnal component of the *L* and *S* variations are examined. Both *L* and *S* amplitudes correlate with the solar activity index $F_{10.7}$, revealing a prominent 11 year solar cycle. In both cases, the correlation is slightly better with $\sqrt{F_{10.7}}$ than $F_{10.7}$. The sensitivity of the *L* variation to solar activity is comparable with that of the *S* variation. The solar cycle effect is also found in the phase of the *S* variation but not apparent in the phase of the *L* variation. The ratio in the amplitude of the *L* to *S* variation shows a long-term decrease (approximately 10% per century), which may be due to a reduction in lunar tidal waves from the lower atmosphere to the upper atmosphere in association with climate change.

1. Introduction

When solar-terrestrial disturbances are absent, records of the Earth's magnetic field on the ground show regular daily variations, which are primarily composed of 24, 12, 8, and 6 h spectral components. Those variations are commonly known as solar quiet (*Sq*) variations [*Chapman and Bartels*, 1940; *Matsushita*, 1967; *Campbell*, 2003]. It is well understood that *Sq* variations are a consequence of electric currents flowing in the dynamo region of the ionosphere (between approximately 90 and 150 km), where the neutral wind drives a electromotive force through the ionospheric wind dynamo mechanism [*Richmond*, 1995a; *Richmond and Maute*, 2014]. During high geomagnetic activity periods, magnetic signatures tend to be dominated by the effect of other currents such as magnetospheric ring currents, but the ionospheric wind-dynamo current system persists to produce *Sq* variations [*Briggs*, 1984; *Hibberd*, 1985].

Changes in *Sq* variations are generally interpreted in terms of these three variables: neutral wind, plasma density, and main geomagnetic field in the dynamo region. Driving winds for the currents responsible for *Sq* variations are atmospheric solar tides that are generated locally in the thermosphere due to solar ultraviolet heating [*Stening*, 1969; *Tarpley*, 1970a; *Takeda and Maeda*, 1980]. Besides, solar tidal waves from the lower atmosphere also play a significant role in driving the wind dynamo currents [*Richmond and Roble*, 1987; *Yamazaki et al.*, 2014]. Satellite measurements of solar tides in the dynamo region can be found in the literature [*McLandress et al.*, 1996; *Forbes et al.*, 2008]. Another important parameter for *Sq* currents is the electrical conductivity of the ionosphere. Ionospheric conductivities vary with the ionospheric plasma density, as well as the strength of the Earth's main magnetic field *Takeda and Araki* [1985].

Long-term changes in *Sq* variations have been studied by many authors. It is well known that the magnitude of *Sq* variations increases with increasing sunspot number [*Chapman and Bartels*, 1940, and references therein]. The midlatitude *Sq* current intensity during solar maximum is approximately twice as high as that during solar minimum [*Takeda*, 1999, 2002]. The amplitude and phase of seasonal *Sq* variations are also modulated by solar activity [*Yamazaki and Yumoto*, 2012; *Çelik et al.*, 2012]. The solar activity dependence of *Sq* variations is mainly due to enhanced ionospheric conductivities during high solar activity periods, which lead to increased ionospheric currents [*Takeda et al.*, 2003]. Also, the high-latitude electric field, driven by the magnetospheric dynamo, is enhanced during high solar activity periods, which leaks to lower latitudes and affects *Sq* currents [*Zaka et al.*, 2010]. The effect of solar activity on *Sq* variations is evident even on time scales longer than a solar cycle (~11 years). *Le Mouël et al.* [2005] and *Macmillan and Droujinina* [2007], using an 11 year running average, demonstrated how closely long-term changes in the magnitude of *Sq* variations follow long-term changes in solar radiation activity.

In order to determine long-term *Sq* changes other than those caused by solar activity, some authors attempted to "remove" the effect of solar activity by fitting solar activity indices, such as sunspot number, and subtract the fit from the original data. *Sellek* [1980] and *Schlapp et al.* [1990] examined the residual *Sq* amplitude after subtraction of the linear fit to the sunspot number. They found significant trends in the residual at some stations, but the trends were not always consistent among stations. *Elias et al.* [2010], conducting a similar analysis, showed increasing trends in the residuals at Apia (13.8°S, 188.2°E), Fredericksburg (38.2°N, 282.6°E), and Hermanus (34.4°S, 19.2°E) during 1960–2001. They argued that the observed increasing trends are partly due to an increase of CO_2 as well as a secular decrease in the main geomagnetic field strength. Earlier, *Rishbeth and Roble* [1992], using a numerical model, predicted that an increase in the CO_2 concentration would lead to an increase of the plasma density at dynamo region altitudes. *Jarvis* [2005], on the contrary, found a long-term decrease in the diurnal and semidiurnal spectral power at Lerwick (61.1°N, 358.8°E), Niemegk (52.1°N, 12.7°E), and Tucson (32.2°N, 249.3°E) after removing components correlated with the sunspot number and *aa* index. The long-term reduction was attributed to a long-term reduction in the solar diurnal and semidiurnal tides from the lower atmosphere, which was reported earlier by *Bremer et al.* [1997] based on wind measurements. The reduction in tidal forcing from the lower atmosphere was predicted to occur by *Ross and Walterscheid* [1991] in connection with a depletion of stratospheric ozone. *de Haro Barbas et al.* [2013], by carefully comparing the residual *Sq* trends at Apia, Fredericksburg, Hermanus, Bangui (4.4°S, 18.6°E), and Trivandrum (8.5°N, 77.0°E) with model results, suggested that the secular variation of the main geomagnetic field is the primary source of long-term *Sq* changes at those stations.

Besides solar daily variations, ground geomagnetic perturbations also show lunar spectral components. The main component is the semidiurnal lunar variation with a period of 12 h in lunar time, or ~12.42 h in solar time. The geomagnetic lunar (*L*) variation is usually much smaller than the geomagnetic solar (*S*) variation, approximately one tenth in magnitude [*Yamazaki et al.*, 2011]. Atmospheric lunar tides are responsible for the ionospheric currents that produce the *L* variations on the ground [*Maeda and Fujiwara*, 1967; *Tarpley*, 1970b]. Lunar tidal waves are excited near the surface due to the gravitational forcing of the Moon acting on the lower atmosphere, solid Earth, and ocean [*Lindzen and Chapman*, 1969; *Hollingsworth*, 1971]. Those waves can propagate vertically upward into the ionospheric dynamo region, just as upward propagating solar tides do. In the dynamo region, the lunar semidiurnal tide in the wind attains the amplitude of up to 10–15 m s^{-1} [*Stening et al.*, 1994; *Zhang and Forbes*, 2013; *Forbes et al.*, 2013], which is smaller than the solar semidiurnal tide by a factor of 3–5 at the same level. Despite its relatively small amplitude, atmospheric lunar tides have been extensively studied in the past. The primary reason for this is the fact that the lunar tidal forcing is, in principle, very well known unlike forcing for other atmospheric waves. Therefore, for example, observations of the atmospheric response to lunar tidal periods serve as an excellent test for general circulation models that incorporate the lunar tidal forcing [*Vial and Forbes*, 1994; *Pedatella et al.*, 2012a].

Lunar tidal effects on the upper atmosphere have received renewed attention lately, in the context of vertical atmospheric coupling during stratospheric sudden warming (SSW) events. Observations have indicated enhanced semidiurnal lunar tidal perturbations in the geomagnetic field during SSW events [*Fejer et al.*, 2010; *Park et al.*, 2012; *Yamazaki et al.*, 2012a, 2012b]. At the magnetic equator, the amplitude of *L* variations during SSWs is more than twice as large as that during non-SSW periods [*Yamazaki*, 2013]. Significant changes were also found in *S* variations at midlatitudes [*Yamazaki et al.*, 2012c]. Numerical studies have shown that changes in the background atmosphere during SSWs provide conditions favorable for amplification of lunar and solar semidiurnal tidal waves from the lower atmosphere [e.g., *Stening et al.*, 1997; *Pedatella et al.*, 2012b, 2014; *Forbes and Zhang*, 2012; *Jin et al.*, 2012; *Wang et al.*, 2014]. Those studies demonstrated how changes in the lower atmosphere can drive upper atmospheric variability through lunar and solar semidiurnal tidal waves, which transfer energy and momentum from the lower atmosphere to the upper atmosphere.

In contrast to the *S* variation, long-term changes in the *L* variation have not been studied much. The dependence of the *L* variation on solar activity is known as in the *S* variation. *Chapman et al.* [1971] and *Malin et al.* [1975] reported that the sensitivity of the *L* variation to the sunspot number is significantly smaller than that of the *S* variation, from which they argued that ionospheric currents responsible for the *L* and *S* variations may flow at different levels of the ionosphere. They considered that *L* currents may flow in the *F* region. *Stening and Winch* [1979] noted that the effect of solar activity on the *L* variation varies for different stations and for different periods. *Butcher* [1980] and *Matsushita and Xu* [1984] discussed that *L* currents flowing in the *F* region is improbable, and both *L* and *S* currents should flow primarily in the ionospheric dynamo

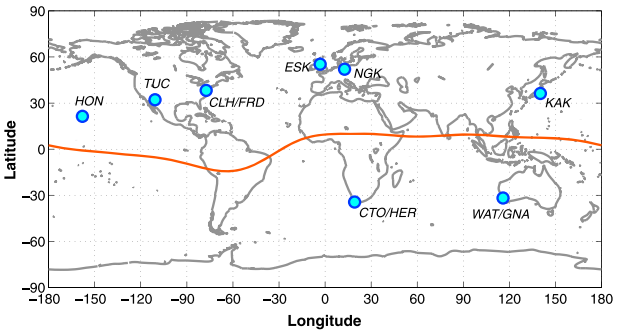

Figure 1. A map of the stations used in the study.

region. Later, *De Meyer* [2003], carefully analyzing *L* and *S* variations at Dourbes (50.1°N, 4.6°E), concluded that the influence of the solar cycle on *L* and *S* variations is nearly the same. Changes in the *L* variation on time scales longer than a solar cycle are far less known.

In this study, geomagnetic data during the last 100 years are analyzed to shed light on long-term changes in both *L* and *S* variations. We examine the semidiurnal component of *L* and *S* variations, focusing on long-term changes on time scales of a solar cycle and longer. Similarities and differences between the two variations are discussed.

2. Data and Methods

Hourly mean data of the geomagnetic field were obtained from the World Data Center for Geomagnetism (Edinburgh). The data from eight midlatitude stations located within ±60° latitude during 1903–2012 were analyzed. The location of the stations and their coordinates are shown in Figure 1 and Table 1, respectively. We use the eastward *Y* component. In previous studies of long-term *Sq* variations, the northward *X* component (or horizontal *H* component) was preferred for no obvious reason [*Jarvis*, 2005; *Elias et al.*, 2010; *de Haro Barbas et al.*, 2013]. At midlatitudes, the vertical *Z* component is the most robust to geomagnetic disturbances among the three components of the geomagnetic field, *X*, *Y*, and *Z* [e.g., *Yamada*, 2002]. The *Z* component is, however, strongly subject to the effect of currents induced in the ocean and conducting Earth, which depends on the exact location of observatories [e.g., *Kuvshinov and Utada*, 2010]. *Takeda* [2013a] demonstrated how long-term variations in *Sq*(*Z*) can be influenced by relocation of an observatory. The effect of geomagnetic activity is most evident in *X* at midlatitudes. Moreover, *Sq*(*X*) is very sensitive to the center position of the *Sq* current whorl, which varies significantly from day to day [*Stening et al.*, 2005a, 2005b] and season to season [*Campbell and Schiffmacher*, 1985, 1988]. *Sq*(*Y*) is much more robust to spatial changes of the overhead current system as well as changes in geomagnetic activity. Hence, the *Y* component is used in this study. The *X* or *H* component could be also used if the effect of magnetospheric ring currents is properly evaluated using the *Dst* index and removed [e.g., *Takeda*, 1984]. However, the *Dst* index can go back only about 50 years, and thus, we did not attempt to analyze the *X* or *H* component in this study.

A 60 day running median value was subtracted from each hourly data point, which removes the secular variation of the main geomagnetic field as well as the effect of magnetospheric currents. The latter can change seasonally [*Campbell*, 2003; *Maus and Lühr*, 2005]. The residual was defined as ΔY. ΔY was visually

Table 1. Observatory Locations[a]

No.	Station	Code	G.Lat.(°N)	G.Lon.(°E)	M.Lat.(°N)	Data Series
1	Eskdalemuir	ESK	55.3	356.8	53.7	1911–2012
2	Niemegk	NGK	52.1	12.7	48.2	1903–2012
3	Fredericksburg	FRD	38.2	282.6	51.2	1956–2011
	Cheltenham	CLH	38.7	283.2		1903–1955
4	Kakioka	KAK	36.2	140.2	28.8	1913–2012
5	Tucson	TUC	32.2	249.3	39.5	1910–2011
6	Honolulu	HON	21.3	202.0	21.6	1903–2011
7	Gnangara	GNA	−31.8	115.9	−43.8	1959–2012
	Watheroo	WAT	−30.3	115.9		1919–1958
8	Hermanus	HER	−34.4	19.2	−41.4	1941–2012
	Cape Town	CTO	−34.0	18.5		1933–1940

[a]G.Lat. and G.Lon. denote geographical latitude and longitude, respectively. M.Lat. denotes magnetic latitude in the magnetic apex coordinate system [*Richmond*, 1995b] as of the year 1958.

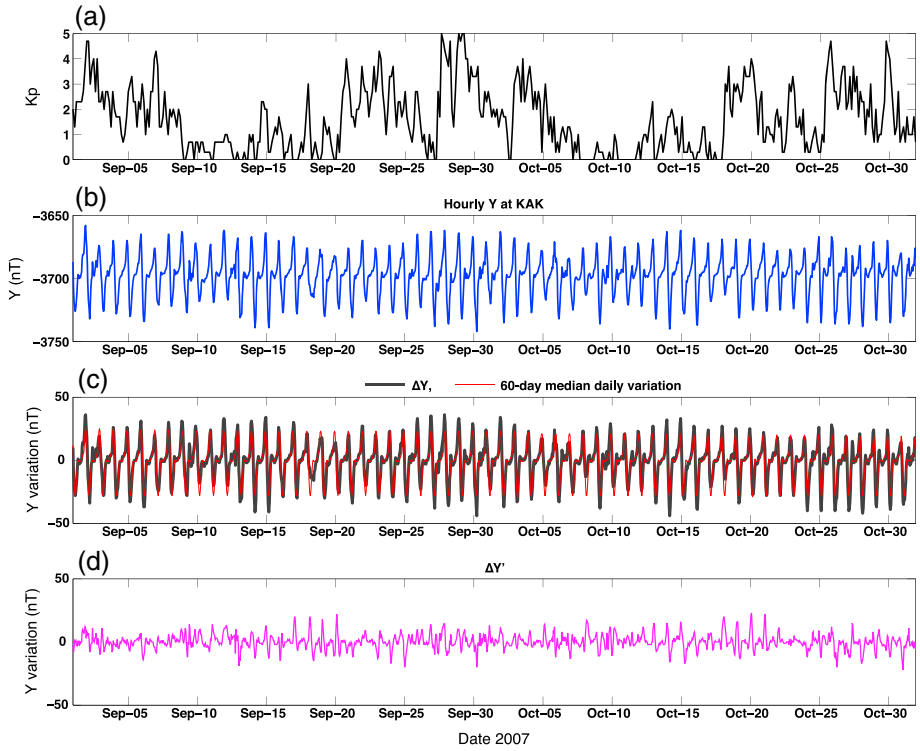

Figure 2. Time series of (a) the geomagnetic activity index *Kp*, (b) *Y* component geomagnetic field at Kakioka, (c) ΔY and 60 day median daily variation, and (d) $\Delta Y'$ for September and October 2007.

inspected, and erroneous data were removed. By erroneous data, we mean extreme values that are certainly artifacts. Also, ΔY that exceeds five standard deviations was automatically rejected for each year, which eliminates the data during severe geomagnetic disturbances. For each solar day, a 60 day median daily variation was determined (i.e., the 60 day running median at each solar hour) and subtracted from ΔY, which removes a substantial portion of the *S* variation. The residual was denoted as $\Delta Y'$. The procedure described above is illustrated in Figure 2 using an example of the *Y* component geomagnetic field at Kakioka during September–October 2007. The main geomagnetic field in the *Y* component is approximately −3700 nT at Kakioka, which can be seen in Figure 2b. The subtraction of the 60 day median baseline gives ΔY, which varies around zero as shown in Figure 2c. Figure 2c also shows the 60 day median daily variation. The deviation of ΔY from the 60 day median daily variation is $\Delta Y'$, which is plotted in Figure 2d. Figure 2a presents geomagnetic activity index *Kp*. The robustness of the *Y* component to geomagnetic activity can be seen.

L and *S* semidiurnal variations were derived from $\Delta Y'$ and ΔY, respectively, in the following way. For each year, ΔY and $\Delta Y'$ were grouped into three seasons: D months, E months, and J months. The D months are from November of the previous year to February. The E months are March, April, September, and October. The J months are from June to August. This seasonal binning was needed because the phase of *L* and *S* variations varies with seasons. For each seasonal group of the data, *L* and *S* semidiurnal variations were derived from $\Delta Y'$ and ΔY, respectively, using a least squares fitting technique. The *L* and *S* semidiurnal variations are expressed as follows:

$$L_{12} = A_L \cos\left[2(\tau - P_L)\frac{2\pi}{24}\right] \quad (1)$$

$$S_{12} = A_S \cos\left[2(t - P_S)\frac{2\pi}{24}\right] \quad (2)$$

where τ is lunar time in hour; t is solar time (or local time) in hour; A_L and A_S are the amplitude of *L* and *S* semidiurnal variations in nano tesla, respectively; and P_L and P_S are the corresponding phases (i.e., lunar or solar time of maximum in hour). In equations (1) and (2), *L* and *S* variations differ only by the periodicity, which makes the comparison between *L* and *S* variations simple and straightforward. The amplitude and

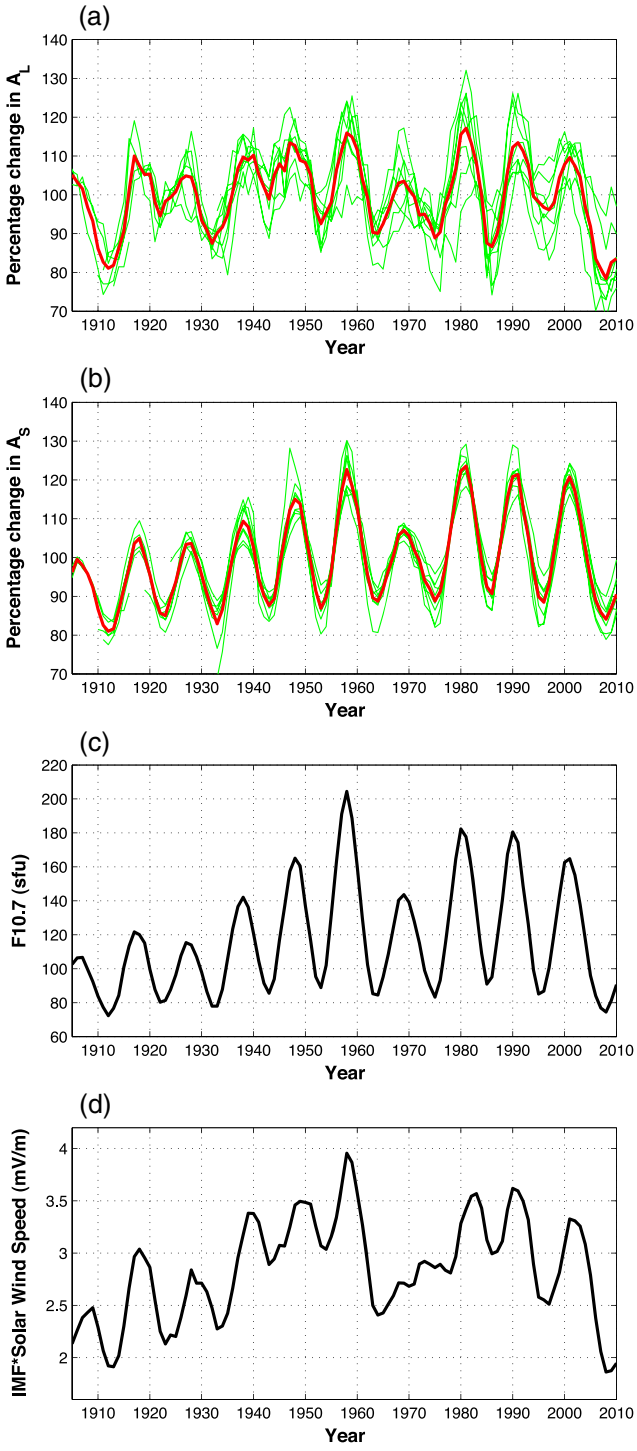

Figure 3. Percent changes in the 5 year averaged amplitude of the (a) *L* variation and (b) *S* variation for 1905–2010. The green lines indicate the results for each station, and the red line indicates their average. The 5 year average of the (c) solar activity index $F_{10.7}$ and (d) interplanetary electric field *BV* is also shown.

phase of the semidiurnal variations were averaged over running 5 years including the preceding and following 2 years. This time window is long enough to reduce the standard error of the small *L* variation sufficiently below its amplitude. We do not examine long-term changes for different seasons separately, which would reduce the amount of data and thus require a longer time average.

3. Results

Figure 3a shows percent changes in the amplitude of the *L* semidiurnal variation from 1905 to 2010. By percent change, we mean the relative change from the average for the whole period. The average *L* semidiurnal amplitude varies between stations, taking values between 1.1 and 2.0 nT (inclusive). The green lines indicate the results from each station, and the red line is their average. The variations are largely similar at different stations, indicating that long-term variations are dominated by global changes. This is also the case for the amplitude of the *S* variation, depicted in Figure 3b. The average *S* semidiurnal amplitude varies between 8.9 and 12.9 nT (inclusive) for different stations.

The 11 year solar cycle can be clearly seen in both Figures 3a and 3b. The *L* and *S* amplitudes change approximately ±20% due to the solar cycle variation. Given that our results are 5 year averaged, the actual year-to-year response of the *L* and *S* variations to the solar cycle would be greater. It is important to note that the sensitivity of the *L* variation to the solar cycle is comparable with that of the *S* variation, which does not support the claim by previous researchers that the *S* variation is 2–3 times more sensitive to the solar cycle [*Chapman et al.*, 1971; *Malin et al.*, 1975; *Olsen*, 1993]. Indeed, a later study found that the sensitivity of *L* and *S* variations to the sunspot number is nearly the same [*De Meyer*, 2003]. It can be seen in the figures that changes in the *L* and *S* amplitudes differs in detail. The difference will be discussed in section 4.

We plot in Figure 3c the 5 year average of the solar radiation index $F_{10.7}$ during

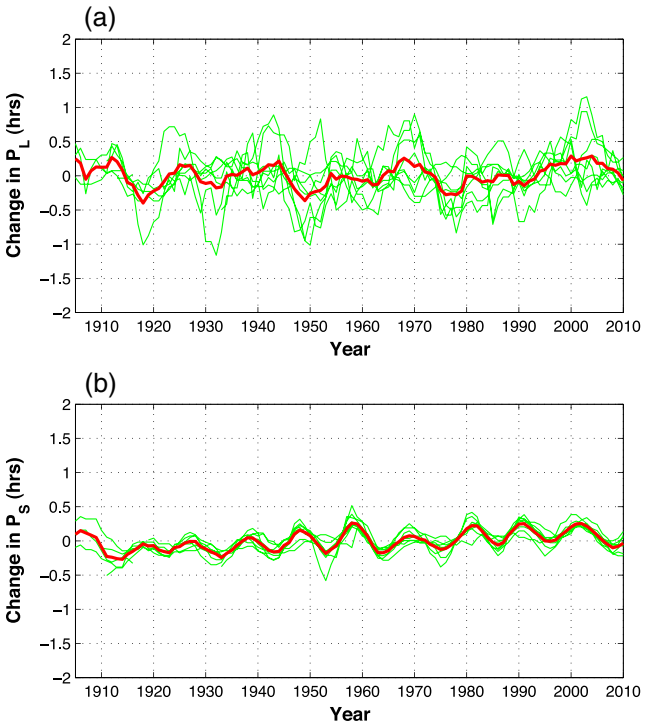

Figure 4. Changes in the 5 year averaged phase of the (a) *L* variation and (b) *S* variation for 1905–2010. The green lines are for each station, and the red line is for their average.

1905–2010. The $F_{10.7}$ index is a good proxy for the solar extreme ultraviolet (EUV) radiation flux, which creates ionospheric plasma. The data before 1948 are derived from the sunspot number using the following formula given by *Tapping et al.* [2007]:

$$F_{10.7} = \frac{N_S}{2}\left[2 - \exp\left(-0.01 N_S\right)\right] \qquad (3)$$

where N_S is annually averaged values of the sunspot number. The $F_{10.7}$ index was provided by the Herzberg Institute of Astrophysics for 1948 and onward. The correlation is remarkable between the $F_{10.7}$ index and the *S* variation amplitude. The square of the correlation coefficient R^2 gives a measure of the goodness of the linear fit. We found $R^2 = 0.94$ for $F_{10.7}$ and A_S (average of all stations). The correlation is slightly better when $\sqrt{F_{10.7}}$ is used, which gives $R^2 = 0.95$. This is the case for all stations, i.e., the correlation is better when $\sqrt{F_{10.7}}$ is used, although the difference in R^2 is small. For the amplitude of the *L* variation (average of all stations), we obtained $R^2 = 0.68$ for $F_{10.7}$ and $R^2 = 0.70$ for $\sqrt{F_{10.7}}$. The use of $\sqrt{F_{10.7}}$ yields a better correlation than $F_{10.7}$ at all stations. We will discuss later in section 4 why $\sqrt{F_{10.7}}$ tends to fit better than $F_{10.7}$ to both *L* and *S* amplitudes.

Figure 3d shows the 5 year average of the interplanetary electric field *BV*, which dominates the high-latitude electric field. *B* is the magnitude of the interplanetary magnetic field (IMF), and *V* is the solar wind speed. Strictly speaking, the high-latitude electric field is controlled by the IMF clock angle as well [*Shepherd et al.*, 2002]. However, the dependence on the IMF clock angle becomes negligible on time scales of yearly average [*Lockwood et al.*, 2013], which justifies the use of *BV* as a measure of the solar wind effect on the high-latitude electric field. The solar wind parameters before 1965 are estimated from geomagnetic activity by *Svalgaard and Cliver* [2007, 2010], while they are from satellite data in the OMNI database [*King and Papitashvili*, 2005] for 1965 and onward. (It is noted that an updated version of the *BV* estimate from geomagnetic activity was recently made available by *Lockwood et al.* [2014].) The variations in $F_{10.7}$ and *BV* are similar not only for the 11 year solar cycle but also for a longer-period variation, which is characterized by a steady increase from the beginning through 1950s, a local minimum around 1965, and a declining trend since 1980s. Those long-term variations can be found in the *L* and *S* amplitudes as well. A correlation analysis reveals $R^2 = 0.58$ for *BV* and A_S, and $R^2 = 0.57$ for *BV* and A_L.

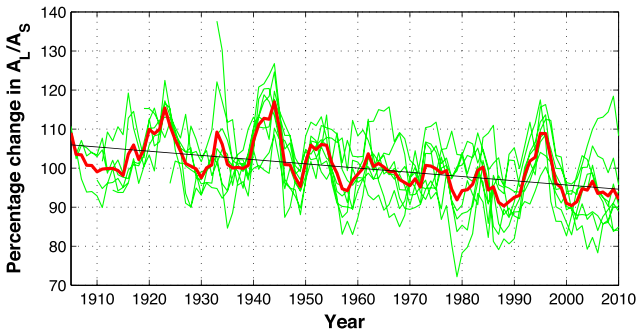

Figure 5. Percent changes in the 5 year averaged lunar-to-solar amplitude ratio for 1905–2010. The green lines are for each station, and the red line is for their average. The black line indicates the linear trend in the average (red). The trends at each station and the trend in the average are summarized in Table 2.

Long-term changes in the phase of the *L* and *S* variations are depicted in Figure 4. It is noted that the results are 5 year

Table 2. Long-Term Trends in A_L/A_S and Their 95% Confidence Interval

Station Code (From North to South)	Trend[a] (% Per Century)	95% Confidence Interval
ESK	**−9.9**	(−18.3, −4.8)
NGK	2.2	(−3.0, 7.2)
FRD/CLH	**−13.3**	(−17.6, −9.1)
KAK	**−12.5**	(−19.5, −6.3)
TUC	**−13.7**	(−18.7, −9.1)
HON	**−14.1**	(−18.3, −410.0)
GNA/WAT	**−21.2**	(−426.0, −16.5)
HER/CTO	**−23.4**	(−34.7, −12.2)
Trend in the average	**−10.8**	(−13.7, −7.8)

[a]Significant trends are indicated by bold font.

averaged, so that the actual year-to-year variability would be somewhat larger. The figure shows only deviations from the average value at each station. It can be seen that the phases are fairly stable during the period analyzed. For the results averaged for all stations (red), the maximum deviation is less than 1 h. The 11 year solar cycle is visible in the phase of the *S* variation. The results for the *L* variation are more noisy, and the solar cycle variation is not apparent. It is known that the focus of the *Sq* current system moves to later local times during solar maximum [*Olsen*, 1993], which produces the solar cycle variation in the phase of the *S* variation. The physical mechanism is yet to be investigated.

Figure 5 shows the ratio in the amplitude of *L* to *S* semidiurnal variation during 1905–2010. It can be seen that the amplitude ratio tends to increase with decreasing solar activity. Besides the 11 year solar cycle, the amplitude ratio also reveals a persistent decrease throughout the period. The lunar-to-solar ratio in 2010 is approximately 10% lower than that of a hundred years ago. The long-term decrease in the lunar-to-solar ratio is largely monotonic (i.e., there is no apparent change in the rate of the decrease), and it is distinct from the long-term trends in $F_{10.7}$ and *BV*, which show rises and falls (Figures 3c and 3d). The long-term trends at individual stations as well as the trend in the average are listed in Table 2, which includes the 95% confidence interval derived using a bootstrap method with 1000 iterations. The long-term reduction is significant (>95%) at all the stations except Niemegk, where the trend is small and insignificant. The ratio of the reduction is found to be greater in the Southern Hemisphere than in the Northern Hemisphere.

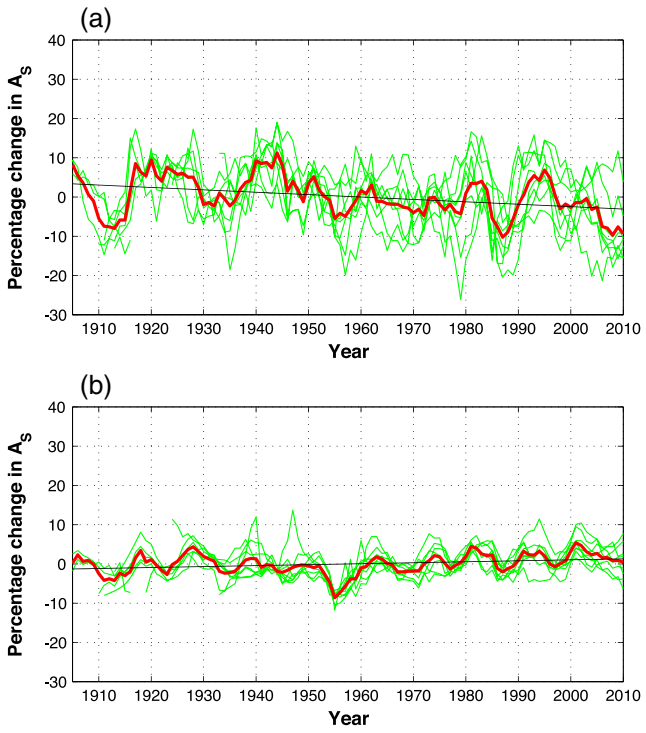

Figure 6. Percent changes in the residual of the 5 year averaged amplitude for the (a) *L* variation and (b) *S* variation after subtraction of the linear fit of $\sqrt{F_{10.7}}$. The green lines are for each station, and the red line is for their average. The black lines show the trend in the average (red). The trends at each station and the trend in the average are summarized in Table 3.

To provide insight into whether the long-term reduction in the lunar-to-solar ratio is due to changes in the *L* variation or *S* variation (or both), we analyzed the long-term trend in the *L* and *S* amplitudes separately. Since we found that both A_L and A_S correlate slightly better with $\sqrt{F_{10.7}}$ than $F_{10.7}$, we use the linear fit of $\sqrt{F_{10.7}}$ to A_L and A_S as a measure of the solar activity influence on the *L* and *S* variations, respectively. The fitting was made separately for A_L and A_S at each station. We subtracted

Table 3. Long-Term Trends in Residual A_L and A_S

Station Code	Trend in A_L[a] (% Per Century)	Trend in A_S[a] (% Per Century)
ESK	2.0	**8.9**
NGK	2.9	−1.2
FRD/CLH	**−12.2**	0.4
KAK	**−12.1**	1.3
TUC	**−8.2**	**4.2**
HON	**−6.4**	**4.8**
GNA/WAT	**−15.3**	2.4
HER/CTO	**−13.0**	**8.5**
Trend in the average	**−6.1**	**2.5**

[a]Significant trends are indicated by bold font.

those fits from the original A_L and A_S. Variations in the residuals are presented in Figure 6. The green lines indicate the results from each station, and the red line is their average. The trends at individual stations and the trend of the average can be found in Table 3. At most stations, the declining trend in the *L* amplitude is significant. Meanwhile, the trend in the *S* amplitude is positive at most stations, and some of them are significant (>95%). These results indicate that the long-term reduction in A_L/A_S is mainly due to the reduction in A_L. The increase in A_S also contributes but to a smaller extent.

4. Discussion

The interpretation of geomagnetic variations is sometimes complicated by the fact that various processes are involved in changes of ionospheric currents. We take a rather simplified view of *Takeda* [2013b] in order to understand our observational results. *Takeda* [2013b] used a very simple expression for the magnitude (*A*) of the *Y* component geomagnetic daily variation on the basis of *Fukushima*'s [1979] model:

$$A = \frac{3}{4}\mu_0 \Sigma U B_z \tag{4}$$

where μ_0 is the permeability of the vacuum ($= 4\pi \times 10^7$), Σ is the effective ionospheric conductivity (S), *U* is zonal neutral wind speed (m s^{-1}), and B_z is the vertical geomagnetic field strength (nT). The constant 3/4 arises from the fact that the geomagnetic daily variation is produced not only by ionospheric currents but also by currents induced in the conductive Earth, which accounts for approximately 25% of the total effect. In light that the midlatitude ionospheric current system is subject to the Cowling effect [*Takeda*, 1991], the effective ionospheric conductivity is given as follows:

$$\Sigma = \Sigma_P + \frac{\Sigma_H^2}{\Sigma_P} \tag{5}$$

where Σ_P and Σ_H are height-integrated Pedersen and Hall conductivities, respectively. *Takeda* [2013b] computed Σ_P and Σ_H using the International Reference Ionosphere model [*Bilitza*, 1990; *Bilitza et al.*, 2011]. He pointed out that the solar cycle variation in *A* is almost solely due to changes in Σ.

4.1. Correlation of $F_{10.7}$ With *L* and *S* Variations

It is found that both lunar and solar variations correlate slightly better with $\sqrt{F_{10.7}}$ than $F_{10.7}$. According to *Takeda* [2013b], Pedersen and Hall conductivities at a given height are proportional to the electron number density N_e. The electron number density tends to scale with $\sqrt{F_{10.7}}$ in the dynamo region where the ionospheric plasma is largely in photochemical equilibrium. The dominant plasma species is O_2^+, which is produced by photoionization at a rate *J* (s^{-1}) and lost through recombination with electrons at a rate α (s^{-1}). That is,

$$O_2 + h\nu \xrightarrow{J} O_2^+ + e^- \tag{6}$$

$$O_2^+ + e^- \xrightarrow{\alpha} O + O \tag{7}$$

where ν represents an EUV photon. Photochemical equilibrium implies the following:

$$J N_{O_2} = \alpha N_{O_2^+} N_e \tag{8}$$

$$\approx \alpha N_e^2 \tag{9}$$

where N_{O_2} and $N_{O_2^+}$ are number densities of O_2 and O_2^+, respectively. Therefore, the electron number density N_e tends to change with $\sqrt{J}$, or $\sqrt{F_{10.7}}$ if the EUV flux is proportional to $F_{10.7}$.

4.2. Differences in the Solar Cycle Response of *L* and *S* Variations

We found differences in the solar cycle response of *L* and *S* variations (Figures 3a and 3b). There are solar minimum periods when the *L* amplitude does not decrease as much as the *S* amplitude does, e.g., 1923, 1944, and 1996. It is possible that the *L* amplitudes for these years are dominated by the effect of SSWs, which significantly enhances *L* variations. Although the occurrence of SSWs is basically limited to the northern winter periods, the effect on *L* variations is strong enough to affect its yearly average amplitude [*Yamazaki*, 2013]. *Yamazaki* [2013] identified the occurrence of SSWs for the years 1994, 1995, 1997, and 1998. Since we use 5 year averaged amplitudes, A_L around the year 1996 should be under significant influence of these SSWs. We could not confirm whether the *L* amplitudes for 1923 and 1944 are also affected by SSWs, because there is no stratospheric data to identify the occurrence of SSWs for these periods. There is indirect evidence to suggest the occurrence of an SSW for 1923. *Bartels and Johnston* [1940] reported an extraordinary large *L* variation at the magnetic equator for January 1923. An abnormally enhanced *L* variation at the magnetic equator is often observed during a strong SSW event. SSWs also affect *S* variations but in a different way [*Yamazaki et al.*, 2012c]. Relative changes in *S* during SSWs are, on average, much smaller compared to those in *L* (Y. Yamazaki, Solar and lunar ionospheric electrodynamic effects during stratospheric sudden warmings, submitted to *Journal of Atmospheric and Solar-Terrestrial Physics*, 2014).

There may be other atmospheric processes that modulate year-to-year variability of the *L* amplitude. For example, *Pedatella and Forbes* [2009] and *Pedatella and Liu* [2013] presented evidence that upward propagation of some tides is affected by the El Niño–Southern Oscillation (ENSO). Similarly, the quasi-biennial oscillation (QBO) in the stratosphere and mesosphere has some influence on tidal propagation [*Hagan et al.*, 1992, 1999; *Xu et al.*, 2009]. Indeed, *Olsen* [1994] and *Jarvis* [1996, 1997] reported small but significant QBO signatures in the *S* variation. The effect of ENSO and QBO on the lunar tide, however, has not been studied.

It is likely that the solar cycle effect on the *L* variation presented by earlier researchers is more or less affected by the effect of SSW (and possibly by other atmospheric effects). This is a significant issue when one attempts to determine the sensitivity of the *L* variation to solar activity from a relatively small data set, e.g., a few years respectively from a solar maximum and solar minimum [e.g., *Chapman et al.*, 1971; *Malin et al.*, 1975].

4.3. Solar Cycle Effect on the Lunar-to-Solar Amplitude Ratio

We have shown that the amplitude ratio in the *L* to *S* variation increases with decreasing solar activity (Figure 5). In light of equation (4), *L* and *S* semidiurnal amplitudes may be assumed to be proportional to the effective ionospheric conductivity Σ, zonal neutral wind speed U, and geomagnetic field strength B_z. Designating U_L and U_S as the wind speed for lunar and solar semidiurnal tides, the amplitude ratio in the *L* to *S* variation can be expressed as follows:

$$\frac{A_L}{A_S} \propto \frac{U_L^*}{U_S^* + U_S^\circ} \tag{10}$$

where the asterisks (*) denote the effect of upward propagating tides from the lower atmosphere, while the circle (∘) represents the contribution of the tides locally generated in the dynamo region. Enhanced solar heating during high solar activity periods would lead to greater solar heating in the dynamo region and hence a larger U_S°. Also, there is evidence in the literature [*Bremer et al.*, 1997; *Baumgaertner et al.*, 2005] that solar semidiurnal tides from the lower atmosphere decrease with increasing solar activity. The mechanism for this is not fully understood, but changes in the background atmosphere, and thus changes in the propagation conditions, may be a reason. If that is the case, a similar solar cycle dependence would be expected in upward propagating lunar semidiurnal tides. Therefore, the negative response of A_L/A_S to solar activity can be qualitatively understood as arising from the increased in situ forcing (thus increased U_S°) and decreased lower atmospheric forcing (thus decreased U_L^* and U_S^*) during high solar activity periods.

4.4. Long-Term Changes in *L* and *S* Variations

Our results have revealed a long-term reduction in the amplitude ratio A_L/A_S (Figure 5 and Table 2). This is probably due to a reduction of the lunar tidal wind in the dynamo region. A separate analysis of *L* and *S* variations (Figure 6 and Table 3) has also indicated a negative trend in A_L, while the trend tends to be positive for

A_S. The global-scale centurial increase in the *S* range was also reported by *Svalgaard* [2009]. The long-term increase in the *S* variation can be attributed to an increase in ionospheric conductivities associated with the decrease of the geomagnetic dipole moment. *Takeda* [1996] numerically studied how the strength of the main geomagnetic field affects the ionospheric wind dynamo. *Cnossen and Richmond* [2013], also using a numerical model, described the effect of secular changes in the Earth's magnetic field on *Sq* variations; a comparison with observations was presented later by *de Haro Barbas et al.* [2013]. The *L* variation should be subject to the same effect from the increasing ionospheric conductivities, but a reduction in the lunar tidal wind is probably dominant, so that the net effect produces a declining trend. It is not clear what causes the long-term reduction in the lunar tidal wind.

Climate change in the lower atmosphere has an impact on the upper atmosphere through various mechanisms [*Cnossen*, 2012]. Long-term changes in the atmospheric composition, such as an increase of CO_2, can affect the dynamics of the lower and middle atmosphere, through which lunar tidal waves propagate. Numerical studies will be necessary to gain a better understanding for long-term changes in the lunar tidal wind.

5. Conclusions

We have examined geomagnetic lunar (*L*) and solar (*S*) semidiurnal variations at eight midlatitude stations during 1903–2012. The *L* and *S* variations are a consequence of electric currents flowing in the ionospheric dynamo region between approximately 90 and 150 km, driven by lunar and solar tidal winds, respectively. The following are the main results of the present study:

1. Five year averaged amplitudes of the *L* and *S* semidiurnal variations show prominent 11 year solar cycle variations of approximately ±20%. The sensitivity of the *L* variation to solar activity is comparable with the sensitivity of the *S* variation to solar activity, consistent with the conclusion of *De Meyer* [2003]. Changes in the *L* amplitude can be contaminated by the effect of the stratospheric sudden warming (SSW), as well as other atmospheric effects.
2. Both *L* and *S* amplitudes correlate with the solar activity index $F_{10.7}$. In both cases, the correlation is slightly better with $\sqrt{F_{10.7}}$ than $F_{10.7}$. This is probably due to the fact that the effective ionospheric conductivity tends to be proportional to the electron number density, which scales with the square root of the plasma production rate under photochemical equilibrium.
3. The solar cycle variation is also present in the phase of the *S* semidiurnal variation but not apparent in the *L* variation phase.
4. The ratio in the amplitude of *L* to *S* semidiurnal variation decreases with increasing solar activity. This can arise from an increased in situ forcing and decreased lower atmospheric forcing during high solar activity periods.
5. The lunar-to-solar amplitude ratio also shows a long-term reduction of approximately 10% per century. This is due to a reduction in the *L* amplitude, as well as an increase in the *S* amplitude to a smaller extent. The long-term increase in the *S* amplitude is attributed to an increase in ionospheric conductivities due to the secular variation of the geomagnetic field. The long-term decrease in the *L* amplitude is probably due to a decrease of the lunar tidal wind in the dynamo region, which is possibly linked to climate change in the lower atmosphere.

Acknowledgments
Geomagnetic variation data were obtained from the World Data Centre for Geomagnetism (Edinburgh) Web site. The geomagnetic activity index *Kp* was provided by the German Research Center for Geosciences (GFZ). This work was supported by NERC grant NE/K01207X/1.

Larry Kepko thanks Ana Elias and Ingrid Cnossen for their assistance in evaluating this paper.

References

Bartels, J., and H. F. Johnston (1940), Geomagnetic tides in horizontal intensity at Huancayo, *Terr. Magn. Atmos. Electr.*, *45*, 269–308, doi:10.1029/TE045i003p00269.

Baumgaertner, A. J. M., A. J. McDonald, G. J. Fraser, and G. E. Plank (2005), Long-term observations of mean winds and tides in the upper mesosphere and lower thermosphere above Scott Base, Antarctica, *J. Atmos. Sol. Terr. Phys.*, *67*, 1480–1496.

Bilitza, D. (1990), *International Reference Ionosphere 1990*, NSSDC, Greenbelt, Maryland.

Bilitza, D., L.-A. McKinnell, B. Reinisch, and T. Fuller-Rowell (2011), The International Reference Ionosphere (IRI) today and in the future, *J. Geod.*, *85*, 909–920, doi:10.1007/s00190-010-0427-x.

Bremer, J., R. Schminder, K. M. Greisiger, P. Hoffmann, D. Kurschner, and W. Singer (1997), Solar cycle dependence and long-term trends in the wind field of the mesosphere/lower thermosphere, *J. Atmos. Sol. Terr. Phys.*, *59*, 497–509.

Briggs, B. H. (1984), The variability of ionospheric dynamo currents, *J. Atmos. Terr. Phys.*, *46*, 419–429.

Butcher, E. C. (1980), On the location of the ionospheric current systems responsible for the lunar and solar magnetic variations, *Geophys. J. R. Astron. Soc.*, *63*, 775–782.

Campbell, W. H. (2003), *Introduction to Geomagnetic Fields*, 304 pp., Cambridge Univ. Press, New York.

Campbell, W. H., and E. R. Schiffmacher (1985), Quiet ionospheric currents of the northern hemisphere derived from geomagnetic field records, *J. Geophys. Res.*, *90*(A7), 6475–6486, doi:10.1029/JA090iA07p06475.

Campbell, W. H., and E. R. Schiffmacher (1988), Quiet ionospheric currents of the southern hemisphere derived from geomagnetic records, *J. Geophys. Res.*, *93*(A2), 933–944, doi:10.1029/JA093iA02p00933.
Çelik, C., M. K. TunÇer, E. Tolak-Çiftçi, M. Zobu, N. Oshiman, and S. B. Tank (2012), Solar and lunar geomagnetic variations in the northwestern part of Turkey, *Geophys. J. Int.*, *189*, 391–399, doi:10.1111/j.1365-246X.2012.05382.x.
Chapman, S., and J. Bartels (1940), *Geomagnetism*, vol. 1, pp. 214–243, Oxford Univ. Press, Oxford, U. K.
Chapman, S., J. C. Gupta, and S. R. C. Malin (1971), The sunspot cycle influence on the solar and lunar daily geomagnetic variations, *Proc. R. Soc. London, Ser. A*, *324*, 1–15, doi:10.1098/rspa.1971.0124.
Cnossen, I. (2012), Climate change in the upper atmosphere, in *Greenhouse Gases: Emission, Measurement, and Management*, edited by G. Liu, pp. 315–336, InTech, Rijeka, Croatia.
Cnossen, I., and A. D. Richmond (2013), Changes in the Earth's magnetic field over the past century: Effects on the ionosphere-thermosphere system and solar quiet (Sq) magnetic variation, *J. Geophys. Res. Space Physics*, *118*, 849–858, doi:10.1029/2012JA018447.
de Haro Barbas, B. F., A. G. Elias, I. Cnossen, and M. Zossi de Artigas (2013), Long-term changes in solar quiet (Sq) geomagnetic variations related to Earth's magnetic field secular variation, *J. Geophys. Res. Space Physics*, *118*, 3712–3718, doi:10.1002/jgra.50352.
De Meyer, F. (2003), A modulation model for the solar and lunar daily geomagnetic variations, *Earth Planets Space*, *55*, 405–418.
Elias, A. G., M. Zossi de Artigas, and B. F. de Haro Barbas (2010), Trends in the solar quiet geomagnetic field variation linked to the Earth's magnetic field secular variation and increasing concentrations of greenhouse gases, *J. Geophys. Res.*, *115*, A08316, doi:10.1029/2009JA015136.
Fejer, B. G., M. E. Olson, J. L. Chau, C. Stolle, H. Lühr, L. P. Goncharenko, K. Yumoto, and T. Nagatsuma (2010), Lunar-dependent equatorial ionospheric electrodynamic effects during sudden stratospheric warmings, *J. Geophys. Res.*, *115*, A00G03, doi:10.1029/2010JA015273.
Forbes, J. M., and X. Zhang (2012), Lunar tide amplification during the January 2009 stratosphere warming event: Observations and theory, *J. Geophys. Res.*, *117*, A12312, doi:10.1029/2012JA017963.
Forbes, J. M., X. Zhang, S. Palo, J. Russell, C. J. Mertens, and M. Mlynczak (2008), Tidal variability in the ionospheric dynamo region, *J. Geophys. Res.*, *113*, A02310, doi:10.1029/2007JA012737.
Forbes, J. M., X. Zhang, S. Bruinsma, and J. Oberheide (2013), Lunar semidiurnal tide in the thermosphere under solar minimum conditions, *J. Geophys. Res. Space Physics*, *118*, 1788–1801, doi:10.1029/2012JA017962.
Fukushima, N. (1979), Electric potential difference between conjugate points in middle latitudes caused by asymmetric dynamo in the ionosphere, *J. Geomagn. Geoelec.*, *31*, 401–409.
Hagan, M. E., F. Vial, and J. M. Forbes (1992), Variability in the upward propagating semidiurnal tide due to effects of QBO in the lower atmosphere, *J. Atmos. Terr. Phys.*, *54*, 1465–1474.
Hagan, M. E., M. D. Burrage, J. M. Forbes, J. Hackney, W. J. Randel, and X. Zhang (1999), QBO effects on the diurnal tide in the upper atmosphere, *Earth Planets Space*, *51*, 571–578.
Hibberd, F. H. (1985), The geomagnetic S_q variation—Annual, semi-annual and solar cycle variations and ring current effects, *J. Atmos. Terr. Phys.*, *47*, 341–352.
Hollingsworth, A. (1971), The effect of ocean and Earth tides on the semi-diurnal lunar air tide, *J. Atmos. Sci.*, *28*, 1021–1044.
Jarvis, M. J. (1996), Quasi-biennial oscillation effects in the semidiurnal tide of the Antarctic lower thermosphere, *Geophys. Res. Lett.*, *23*, 2661–2664, doi:10.1029/96GL02394.
Jarvis, M. J. (1997), Latitudinal variation of quasi-biennial oscillation modulation of the semidiurnal tide in the lower thermosphere, *J. Geophys. Res.*, *102*(A12), 27,177–27,187, doi:10.1029/97JA02034.
Jarvis, M. J. (2005), Observed tidal variation in the lower thermosphere through the 20th century and the possible implication of ozone depletion, *J. Geophys. Res.*, *110*, A04303, doi:10.1029/2004JA010921.
Jin, H., Y. Miyoshi, D. Pancheva, P. Mukhtarov, H. Fujiwara, and H. Shinagawa (2012), Response of migrating tides to the stratospheric sudden warming in 2009 and their effects on the ionosphere studied by a whole atmosphere-ionosphere model GAIA with COSMIC and TIMED/SABER observations, *J. Geophys. Res.*, *117*, A10323, doi:10.1029/2012JA017650.
King, J. H., and N. E. Papitashvili (2005), Solar wind spatial scales in and comparisons of hourly wind and ACE plasma and magnetic field data, *J. Geophys. Res.*, *110*, A02104, doi:10.1029/2004JA010649.
Kuvshinov, A., and H. Utada (2010), Anomaly of the geomagnetic Sq variation in Japan: Effect from 3-D subterranean structure or the ocean effect?, *Geophys. J. Int.*, *183*, 1239–1247, doi:10.1111/j.1365-246X.2010.04809.x.
Le Mouël, J. L., V. Kossobokov, and V. Courtillot (2005), On long-term variations of simple geomagnetic indices and slow changes in magnetospheric currents: The emergence of anthropogenic global warming after 1990?, *Earth Planet. Sci. Lett.*, *232*, 273–286.
Lindzen, R. S., and S. Chapman (1969), Atmospheric tides, *Space Sci. Rev.*, *10*, 3–188.
Lockwood, M., L. Barnard, H. Nevanlinna, M. J. Owens, R. G. Harrison, A. P. Rouillard, and C. J. Davis (2013), Reconstruction of geomagnetic activity and near-Earth interplanetary conditions over the past 167 yr—Part 2: A new reconstruction of the interplanetary magnetic field, *Ann. Geophys.*, *31*, 1979–1992.
Lockwood, M., H. Nevanlinna, L. Barnard, M. J. Owens, R. G. Harrison, A. P. Rouillard, and C. J. Scott (2014), Reconstruction of geomagnetic activity and near-Earth interplanetary conditions over the past 167 yr—Part 4: Near-earth solar wind speed, IMF, and open solar flux, *Ann. Geophys.*, *32*, 383–399.
Malin, S. R. C., A. Cecere, and A. Palumbo (1975), The sunspot cycle influence on lunar and solar daily geomagnetic variations, *Geophys. J. R. Astron. Soc.*, *41*, 115–126.
Maeda, H., and M. Fujiwara (1967), Lunar ionospheric winds deduced from the dynamo theory of geomagnetic variations, *J. Atmos. Terr. Phys.*, *29*, 917–936.
Macmillan, S., and A. Droujinina (2007), Long-term trends in geomagnetic daily variation, *Earth Planets Space*, *59*, 391–395.
Matsushita, S. (1967), Solar quiet and lunar daily variation fields, in *Physics of Geomagnetic Phenomena*, edited by S. Matsushita and W. H. Campbell, pp. 302–424, Academic Press, Orlando, Fla.
Matsushita, S., and W.-Y. Xu (1984), Seasonal variations of L equivalent current systems, *J. Geophys. Res.*, *89*(A1), 285–294, doi:10.1029/JA089iA01p00285.
Maus, S., and H. Lühr (2005), Signature of the quiet-time magnetospheric magnetic field and its electromagnetic induction in the rotating Earth, *Geophys. J. Int.*, *162*, 755–763, doi:10.1111/j.1365-246X.2005.02691.x.
McLandress, C., G. G. Shepherd, and B. H. Solheim (1996), Satellite observations of thermospheric tides: Results from the wind imaging interferometer on UARS, *J. Geophys. Res.*, *101*(D2), 4093–4114, doi:10.1029/95JD03359.
Olsen, N. (1993), The solar cycle variability of lunar and solar daily geomagnetic variations, *Ann. Geophys.*, *11*, 254–262.
Olsen, N. (1994), A 27-month periodicity in the low latitude geomagnetic field and its connection to the stratospheric QBO, *Geophys. Res. Lett.*, *21*, 1125–1128.

Park, J., H. Lühr, M. Kunze, B. G. Fejer, and K. W. Min (2012), Effect of sudden stratospheric warming on lunar tidal modulation of the equatorial electrojet, *J. Geophys. Res.*, *117*, A03306, doi:10.1029/2011JA017351.

Pedatella, N. M., and J. M. Forbes (2009), Interannual variability in the longitudinal structure of the low-latitude ionosphere due to the El Niño–Southern Oscillation, *J. Geophys. Res.*, *114*, A12316, doi:10.1029/2009JA014494.

Pedatella, N. M., and H.-L. Liu (2013), Influence of the El Niño Southern Oscillation on the middle and upper atmosphere, *J. Geophys. Res. Space Physics*, *118*, 2744–2755, doi:10.1002/jgra.50286.

Pedatella, N. M., H.-L. Liu, and A. D. Richmond (2012a), Atmospheric semidiurnal lunar tide climatology simulated by the whole atmosphere community climate model, *J. Geophys. Res.*, *117*, A06327, doi:10.1029/2012JA017792.

Pedatella, N. M., H.-L. Liu, A. D. Richmond, A. Maute, and T.-W. Fang (2012b), Simulations of solar and lunar tidal variability in the mesosphere and lower thermosphere during sudden stratosphere warmings and their influence on the low-latitude ionosphere, *J. Geophys. Res.*, *117*, A08326, doi:10.1029/2012JA017858.

Pedatella, N. M., H.-L. Liu, F. Sassi, J. Lei, J. L. Chau, and X. Zhang (2014), Ionosphere variability during the 2009 SSW: Influence of the lunar semidiurnal tide and mechanisms producing electron density variability, *J. Geophys. Res. Space Physics*, *119*, 3828–3843, doi:10.1002/2014JA019849.

Richmond, A. D. (1995a), Ionospheric electrodynamics, in *Handbook of Atmospheric Electrodynamic*, vol. 2, edited by H. Volland, pp. 249–290, CRC Press, Boca Raton, Fla.

Richmond, A. D. (1995b), Ionospheric electrodynamics using magnetic apex coordinates, *J. Geomagn. Geoelec.*, *47*, 191–212.

Richmond, A. D., and A. Maute (2014), Ionospheric electrodynamics modeling, in *Modeling the Ionosphere-Thermosphere System,* edited by J. Huba, R. Schunk and G. Khazanov, pp. 57–71, John Wiley, Chichester, U. K., doi:10.1002/9781118704417.ch6.

Richmond, A. D., and R. G. Roble (1987), Electrodynamic effects of the thermospheric winds from the NCAR thermospheric general circulation model, *J. Geophys. Res.*, *92*(A11), 12,365–12,376.

Rishbeth, H., and R. G. Roble (1992), Cooling of the upper atmosphere by enhanced greenhouse gases—Modelling of thermospheric and ionospheric effects, *Planet. Space Sci.*, *40*, 1011–1026, doi:10.1016/0032-0633(92)90141-A.

Ross, M. N., and R. L. Walterscheid (1991), Changes in the solar forced tides caused by stratospheric ozone depletion, *Geophys. Res. Lett.*, *18*, 420–423.

Sellek, R. (1980), Secular trends in daily geomagnetic variations, *J. Atmos. Sol. Terr. Phys.*, *42*, 689–695.

Schlapp, D. M., R. Sellek, and E. C. Butcher (1990), Studies of worldwide secular trends in the solar daily geomagnetic variation, *Geophys. J. Int.*, *100*, 469–475.

Shepherd, S. G., R. A. Greenwald, and J. M. Ruohoniemi (2002), Cross polar cap potentials measured with super dual auroral radar network during quasi-steady solar wind and interplanetary magnetic field conditions, *J. Geophys. Res.*, *107*(A7), 1094, doi:10.1029/2001JA000152.

Stening, R. J. (1969), An assessment of the contributions of various tidal winds to the S_q current system, *Planet. Space Sci.*, *17*, 889–908.

Stening, R. J., and D. E. Winch (1979), Seasonal changes in the global lunar geomagnetic variation, *J. Atmos. Terr. Phys.*, *41*, 311–323.

Stening, R. J., A. H. Manson, C. E. Meek, and R. A. Vincent (1994), Lunar tidal winds at Adelaide and Saskatoon at 80 to 100 km heights: 1985–1990, *J. Geophys. Res.*, *99*(A7), 13,273–13,280, doi:10.1029/94JA00298.

Stening, R. J., J. M. Forbes, M. E. Hagan, and A. D. Richmond (1997), Experiments with a lunar atmospheric tidal model, *J. Geophys. Res.*, *102*(D12), 13,465–13,471, doi:10.1029/97JD00778.

Stening, R., T. Reztsova, D. Ivers, J. Turner, and D. Winch (2005a), A critique of methods of determining the position of the focus of the Sq current system, *J. Geophys. Res.*, *110*, A04305, doi:10.1029/2004JA010784.

Stening, R., T. Reztsova, and L. H. Minh (2005b), Day-to-day changes in the latitudes of the foci of the Sq current system and their relation to equatorial electrojet strength, *J. Geophys. Res.*, *110*, A10308, doi:10.1029/2005JA011219.

Svalgaard, L. (2009), Observatory data: A 170-year Sun-Earth connection, in *Proceedings of the XIIIth IAGA Workshop on Geomagnetic Observatory Instruments, Data Acquisition, and Processing*, edited by J. J. Love, pp. 246–257, U.S. Geol. Surv., Reston, Va.

Svalgaard, L., and E. W. Cliver (2007), Interhourly variability index of geomagnetic activity and its use in deriving the long-term variation of solar wind speed, *J. Geophys. Res.*, *112*, A10111, doi:10.1029/2007JA012437.

Svalgaard, L., and E. W. Cliver (2010), Heliospheric magnetic field 1835–2009, *J. Geophys. Res.*, *115*, A09111, doi:10.1029/2009JA015069.

Tapping, K. F., D. Boteler, P. Charbonneau, A. Crouch, A. Manson, and H. Paquette (2007), Solar magnetic activity and total irradiance since the Maunder minimum, *Sol. Phys.*, *246*, 309–326, doi:10.1007/s11207-007-9047-x.

Takeda, M. (1984), Day-to-day variation of equivalent Sq current system during March 11–26, 1970, *J. Geomagn. Geoelec.*, *36*, 215–228.

Takeda, M. (1991), Role of hall conductivity in the ionospheric dynamo, *J. Geophys. Res.*, *96*(A6), 9755–9759, doi:10.1029/91JA00667.

Takeda, M. (1996), Effects of the strength of the geomagnetic main field strength on the dynamo action in the ionosphere, *J. Geophys. Res.*, *101*(A4), 7875–7880, doi:10.1029/95JA03807.

Takeda, M. (1999), Time variation of global geomagnetic S_q field in 1964 and 1980, *J. Atmos. Sol. Terr. Phys.*, *61*, 765–774.

Takeda, M. (2002), Features of global geomagnetic S_q field from 1980 to 1990, *J. Geophys. Res.*, *107*(A9), 1252, doi:10.1029/2001JA009210.

Takeda, M. (2013a), Difference in seasonal and long-term variations in geomagnetic Sq fields between geomagnetic Y and Z components, *J. Geophys. Res. Space Physics*, *118*, 2522–2526, doi:10.1002/jgra.50128.

Takeda, M. (2013b), Contribution of wind, conductivity, and geomagnetic main field to the variation in the geomagnetic Sq field, *J. Geophys. Res. Space Physics*, *118*, 4516–4522, doi:10.1002/jgra.50386.

Takeda, M., and T. Araki (1985), Electric conductivity of the ionosphere and nocturnal currents, *J. Atmos. Terr. Phys.*, *47*, 601–609.

Takeda, M., and H. Maeda (1980), Three-dimensional structure of ionospheric currents. 1. Currents caused by diurnal tidal winds, *J. Geophys. Res.*, *85*(A12), 6895–6899, doi:10.1029/JA085iA12p06895.

Takeda, M., T. Iyemori, and A. Saito (2003), Relationship between electric field and currents in the ionosphere and the geomagnetic Sq field, *J. Geophys. Res.*, *108*(A5), 1183, doi:10.1029/2002JA009659A5.

Tarpley, J. D. (1970a), The ionospheric wind dynamo–II: Solar tides, *Planet. Space Sci.*, *18*, 1091–1103, doi:10.1016/0032-0633(70)90110-8.

Tarpley, J. D. (1970b), The ionospheric wind dynamo–I: Lunar tide, *Planet. Space Sci.*, *18*, 1075–1090, doi:10.1016/0032-0633(70)90109-1.

Vial, F., and J. M. Forbes (1994), Monthly simulations of the lunar semi-diurnal tide, *J. Atmos. Terr. Phys.*, *56*, 1591–1607.

Wang, H., R. A. Akmaev, T.-W. Fang, T. J. Fuller-Rowell, F. Wu, N. Maruyama, and M. D. Iredell (2014), First forecast of a sudden stratospheric warming with a coupled whole-atmosphere/ionosphere model IDEA, *J. Geophys. Res. Space Physics*, *119*, 2079–2089, doi:10.1002/2013JA019481.

Xu, J., A. K. Smith, H.-L. Liu, W. Yuan, Q. Wu, G. Jiang, M. G. Mlynczak, J. M. Russell III, and S. J. Franke (2009), Seasonal and quasi-biennial variations in the migrating diurnal tide observed by Thermosphere, Ionosphere, Mesosphere, Energetics and Dynamics (TIMED), *J. Geophys. Res.*, *114*, D13107, doi:10.1029/2008JD011298.

Yamada, Y. (2002), 2-day, 3-day, and 5–6-day oscillations of the geomagnetic field detected by principal component analysis, *Earth Planets Space*, *54*, 379–392.

Yamazaki, Y. (2013), Large lunar tidal effects in the equatorial electrojet during northern winter and its relation to stratospheric sudden warming events, *J. Geophys. Res. Space Physics*, *118*, 7268–7271, doi:10.1002/2013JA019215.

Yamazaki, Y., and K. Yumoto (2012), Long-term behavior of annual and semi-annual S_q variations, *Earth Planets Space*, *64*, 417–423.

Yamazaki, Y., et al. (2011), An empirical model of the quiet daily geomagnetic field variation, *J. Geophys. Res.*, *116*, A10312, doi:10.1029/2011JA016487.

Yamazaki, Y., K. Yumoto, D. McNamara, T. Hirooka, T. Uozumi, K. Kitamura, S. Abe, and A. Ikeda (2012a), Ionospheric current system during sudden stratospheric warming events, *J. Geophys. Res.*, *117*, A03334, doi:10.1029/2011JA017453.

Yamazaki, Y., A. D. Richmond, and K. Yumoto (2012b), Stratospheric warmings and the geomagnetic lunar tide: 1958–2007, *J. Geophys. Res.*, *117*, A04301, doi:10.1029/2012JA017514.

Yamazaki, Y., A. D. Richmond, H. Liu, K. Yumoto, and Y. Tanaka (2012c), Sq current system during stratospheric sudden warming events in 2006 and 2009, *J. Geophys. Res.*, *117*, A12313, doi:10.1029/2012JA018116.

Yamazaki, Y., A. D. Richmond, A. Maute, Q. Wu, D. A. Ortland, A. Yoshikawa, I. A. Adimula, B. Rabiu, M. Kunitake, and T. Tsugawa (2014), Ground magnetic effects of the equatorial electrojet simulated by the TIE-GCM driven by TIMED satellite data, *J. Geophys. Res. Space Physics*, *119*, 3150–3161, doi:10.1002/2013JA019487.

Zaka, K. Z., et al. (2010), Simulation of electric field and current during the 11 June 1993 disturbance dynamo event: Comparison with the observations, *J. Geophys. Res.*, *115*, A11307, doi:10.1029/2010JA015417.

Zhang, J. T., and J. M. Forbes (2013), Lunar tidal winds between 80 and 110 km from UARS/HRDI wind measurements, *J. Geophys. Res. Space Physics*, *118*, 5296–5304, doi:10.1002/jgra.50420.